JOURNAL OF CATALYSIS 35, 115–139 (1974)

Identification of the Rate Determining Step in Aging of Supported Metals

B. PULVERMACHER AND E. RUCKENSTEIN*

Department of Chemical Engineering, University of Delaware, Newark, Delaware 19711; and State University of New York at Buffalo, Faculty of Engineering and Applied Sciences, Buffalo, New York 14214

Received December 17, 1973; revised May 9, 1974

Aging of supported metal catalysts may result from the diffusion of metal crystallites on the surface of the support and subsequent sintering of the colliding particles. In the present paper procedures to extract from experimental data information about the rate determining step of the process and its characteristics (diffusion coefficient, rate-of-merging constant) are suggested. The experimental methods discussed include electron microscopy, X-ray line broadening, small angle X-ray scattering, magnetic measurements and static chemisorption. The experimental methods provide some average values of the crystallite size which are sensitive to the form of the size distribution. Using for the size distribution theoretical results valid for diffusion or sintering control criteria are established which compared to experimental data allow a choice among various mechanisms.

NOMENCLATURE

a	Total number of particles per unit surface area of support at $t = 0$ divided by total number of particles per unit surface area of support at $t = t$
b	Dummy variable
b_1, b_2, b_3	Constants independent of time
C	Constant independent of particle size
C_1, C_2, C_3, C_4	Constants independent of time
c_i	Number of particles per unit surface area of support composed of i metal units
D_i	Diffusion coefficient of particle composed of i metal units
D_{ij}	Diffusion coefficient of particle i with respect to particle j
e	Exponent independent of particle size
f	Exponent independent of particle size
$g(x)$	Dimensionless distribution function
K^*	Constant independent of particle size
K_L	Constant in Scherrer equation
$K(v,\tilde{v})$	Second order rate constant
k	Constant independent of particle size
L, $\langle L \rangle$	Mean crystallite dimension
L_W	Mean length of particle size distribution defined by Eq. (26)
l, l_i	Crystallite size in continuous and discrete representation, respectively
l_{vs}	Linear dimension of particle size distribution defined by Eq. (49)

* Present address: State University of New York at Buffalo, Buffalo, NY 14214.

M_0, M_1, M_i	Moments of the dimensionless distribution function $g(x)$
m	Exponent
N, N_0	Total number of crystallites per unit surface area of support for $t = t$ and $t = 0$, respectively
N_1, N_2	Total number of particles at times t_1 and t_2, respectively
N_v	Cumulative distribution in the continuous representation
$n(l,t)$ $n(r,t)$ $n(v,t)$	Continuous density distribution function
$n(v,t)dv$	Number of particles per unit surface area of support having a volume in the range v to $v + dv$
n_i	Number of particles of size l_i
$P(x,t)$	Dimensionless cumulative distribution
R_{ij}	Radius of interaction between two colliding particles containing i and j metal units
R_G, R_{G_0}	Guinier radius for point-shaped X-ray beams at $t = t$ and $t = 0$, respectively
R_{G_L}	Guinier radius for line-shaped X-ray beams
R_{HF}	High field radius from magnetic measurements
R_{LF}	Low field radius from magnetic measurements
R_P, R_{P_L}	Porod radius for point-shaped and line-shaped X-ray beams, respectively
R_{VS}	Volume to surface radius
R_W	Mean radius from X-ray line broadening
$R_{e,t}$	Average radius defined by Eq. (A-1)
r	Radius of particle
r_i	Radius of particle containing i metal units
$\langle r \rangle$	Average radius of particle defined by Eq. (8)
S, S_0	Total exposed surface area of metal per unit surface area of support at $t = t$ and $t = 0$, respectively
S^*	Specific exposed surface area of metal per gram of metal
T	Dimensionless time
T_{xy}	Crystal dimension in the direction perpendicular to the reflecting plane x–y
t	Time of process
v, $\tilde{v}$	Volume of a particle
v_0	Initial average volume of the particles
v_i	Volume of a particle containing i metal units
Δv	Volume increment
v_{G_L}, v_{HF}, v_{LF} v_P, v_{VS}, v_W	Average volumes as measured by different techniques defined in Table 4
x	Dimensionless volume
x_{G_L}, x_{HF}, x_{LF} x_P, x_{VS}, x_W	Dimensionless average volumes
α_{ij}	Reaction rate constant for the merging process of two particles containing i and j metal units
α_s	Surface shape factor
α_v	Volume shape factor
β	Diffraction line breadth
ρ	Density of metal
σ	Standard deviation of the size distribution
σ^*	Standard deviation of the dimensionless size distribution

η	Similarity variable in the continuous representation, dimensionless volume
η_i^*	Similarity variable in the discrete representation
θ'	Small scale time in the diffusion model
$\theta^* = 1$ sec	
λ	X-ray wavelength
μ_m	Moments of similarity distribution defined by Eq. (12)
$\tau_1 = t\alpha_{11}2\pi r_1 N_0$	Dimensionless time in the sintering controlled case
$\tau_2 = \frac{t4\pi D_1 N_0}{\ln[4D_{11}\theta^*/(R_{11})^2]}$	Dimensionless time in the diffusion controlled case
ϕ	Total volume of metal per unit surface area of support
ϕ^*	Dimensionless total volume of metal per unit surface area of support
ψ	Similarity variable in the continuous representation, dimensionless distribution function
ψ^*	Similarity variable in the discrete representation

I. Introduction

Aging of supported metal catalysts may result from the diffusion of metal crystallites on the surface of the support and subsequent sintering of the colliding particles (*1*, *2*). If the time needed for two colliding particles to merge into a single unit is long enough compared to the diffusion time, then the merging process is rate determining and the aging is sintering controlled. Alternatively the aging is diffusion controlled. The migration of crystallites is hindered when they experience strong interactions with some sites of the support or when the crystallite sizes approach the dimensions of the pores. When the migration is hindered, an equilibrium crystallite size distribution may be achieved after a certain time (*2*).

For unhindered migration two limiting situations arise. For diffusion controlled aging the size distribution after a sufficiently long time becomes almost independent of the initial distribution and can be represented by a universal curve in the dimensionless variables $\psi \equiv n(v)\ \phi/N^2$ vs $\eta = Nv/\phi$. For sintering controlled aging, no universal curve in the coordinates (ψ,η) exists for the asymptotic behavior of the size distribution; a family of curves dependent on the supplementary parameters $\tau_1 = \alpha_{11}2\pi r_1 N_0 t$ and $\phi^* = \phi/v_1 N_0$ is obtained instead.

In the following paragraphs situations in which migration is unhindered will be considered only. The goal is to develop procedures for extracting from experimental data information about: (i) the rate determining step of the aging process, and (ii) the magnitude and size dependence of the diffusion coefficient of the crystallites and/or of the rate-of-merging constant. Both physical and chemisorption methods are examined. The methods include: (a) electron microscopy; (b) X-ray line broadening; (c) small angle X-ray scattering; (d) magnetization measurements; and (e) static chemisorption.

Each of the experimental techniques provides some average value of the crystallite size. These averages depend on the size distribution. Because the size distribution and its time dependence are sensitive to the rate determining step of aging, a choice among various mechanisms can be made. In this paper available experimental data are interpreted on the basis of the criteria to be established.

II. Electron Microscopy

In recent years improved electron microscopes have become available and microscopic techniques have been refined to give resolutions higher than 2 Å (*3–6*), and crystallites as small as 4–6 Å have been observed and sized (*3–4*).

Theoretically, the size distribution of metal crystallites can thus be obtained to

include very small crystallite sizes. From this information, any average diameter of the size distribution can be calculated with some accuracy.

Electron microscopy, however, provides a measure of the projected crossectional area of a particle perpendicular to the electron beam. Calculations of average diameters of physical significance, as for example the surface average and volume average diameters can only be obtained with an additional assumption concerning the crystallite shape.

In the following development it will be shown that

a. the whole size distribution,
b. the cumulative size distribution, and
c. the variance of the size distribution

can be used to identify the rate controlling step of the aging process. Information about the diffusion coefficient of the crystallites or about the rate-of-merging constant can be obtained from electron micrographs taken at different times of the aging process.

1. *Size Distribution Used to Identify the Rate Determining Step of the Aging Process*

As shown previously (*2*) the time dependent size distribution $n(v,t)$, where $n(v,t)dv$ is the number of particles per unit surface area of support having a volume in the range v to $v + dv$, can be represented for diffusion control after a short transient period by a unique curve in the coordinates

$$\psi(\eta) = \frac{n(v,t)\phi}{N^2} \tag{1}$$

and

$$\eta = \frac{N(t)}{\phi} v. \tag{2}$$

N is the total number of crystallites per unit surface area of support and ϕ is the total volume of crystallites per unit surface area of support. This unique curve is independent of the initial size distribution. The length of time after which this unique curve is reached depends, however, on the initial distribution, being longer for broad initial distributions. For sintering control, no such unique curve exists and, as will be shown later, after a short transient period

$$\frac{n(v,t)\phi}{N^2} = \psi(\eta,\tau_1,\phi^*).$$

For diffusion controlled aging, the shape of the curve $\psi(\eta)$ has been computed earlier for some cases (*2*). New computations have been carried out for various size dependencies of the diffusion coefficient of the crystallites, and the results are plotted in Fig. 1. The results show that for small values of η and thus small crystallites [see Eq. (2)] the shape of the curve $\psi(\eta)$ depends distinctly on the assumed size dependence of the diffusion coefficient. For large values of η and thus larger crystallites, however, the obtained curves are close to each other.

For sintering control and an initially unisized distribution, the corresponding curves are given in Ref. [(2), Fig. 20]. Figures 2 and 3 of this paper show the results obtained also for sintering control

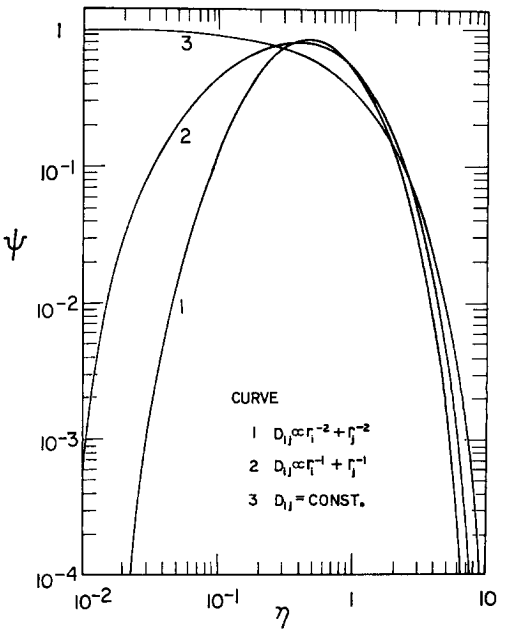

FIG. 1. Similarity solution for diffusion controlled case.

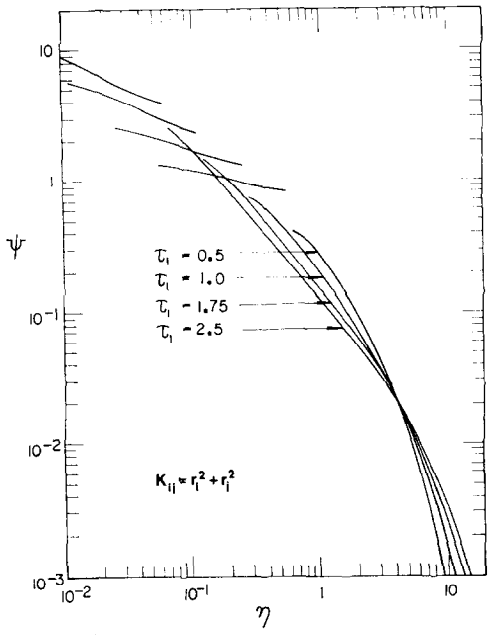

FIG. 2. Similarity solution for sintering controlled case; initial distribution

$$\frac{c_i}{N_0} = \begin{cases} 0.1 & i \leq 10 \\ 0 & i > 10 \end{cases}.$$

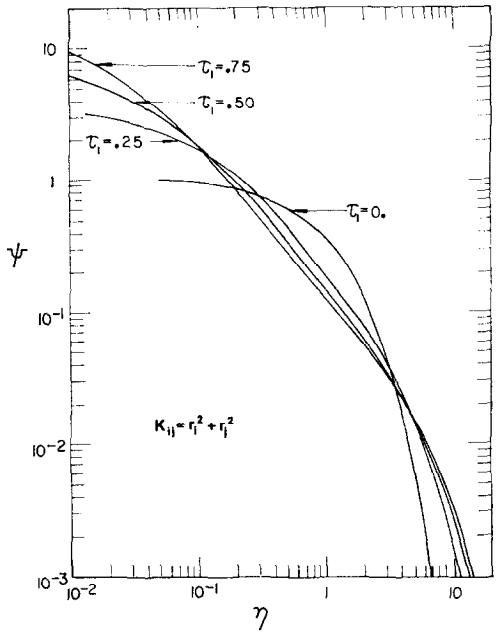

FIG. 3. Similarity solution for sintering controlled case, initial distribution

$$\frac{c_i}{N_0} = \frac{e^{-v_i/20v_1}}{\Sigma_1^{\infty} e^{-v_i/20v_1}}.$$

for two other initial distributions. In all cases a family of curves is obtained which for large sizes exhibit similar shapes even for short times. As time increases, the similarity in shape extends to smaller and smaller sizes. For sufficiently long times a family of curves is obtained: each of them is characterized by the dimensionless time τ_1 and by a constant parameter ϕ^* containing some information about the initial distribution. Since these curves are close to each other, information concerning cumulative distributions and some global characteristics of the size distribution may be obtained using only the similarity variables even in the sintering controlled case.

Comparison of the curves $\psi(\eta)$, obtained for diffusion control, with those obtained for sintering control, [(2), Fig. 20] and Figs. 2 and 3, shows a distinct difference over the whole size range and thus allows differentiation between diffusion and sintering control.

Experiments may furnish a discrete spectrum of crystallite sizes. The discrete version of the variables ψ and η may be taken as

$$\psi^*(\eta_i^*) = \frac{c_i \phi}{N^2 \Delta v}, \tag{4}$$

$$\eta_i^* = \frac{N v_i}{\phi}, \tag{5}$$

where Δv is a volume increment and c_i is the number of particles per unit surface area of support in the volume range $v_i - (\Delta v/2)$ to $v_i + (\Delta v/2)$.

For too large values of Δv, it is difficult to transform the experimentally obtained discrete size distribution into a continuous size distribution. In such a case it is preferable to use a cumulative distribution. The cumulative distribution is defined as $N_v/N = (1/N) \int_v^{\infty} n(v,t)\, dv$ in the continuous representation. For diffusion controlled aging it is, like ψ, dependent only on η:

$$\frac{N_v}{N} = \frac{1}{N} \int_v^{\infty} n(v,t) dv = \int_{\eta}^{\infty} \psi(\eta) d\eta. \tag{6}$$

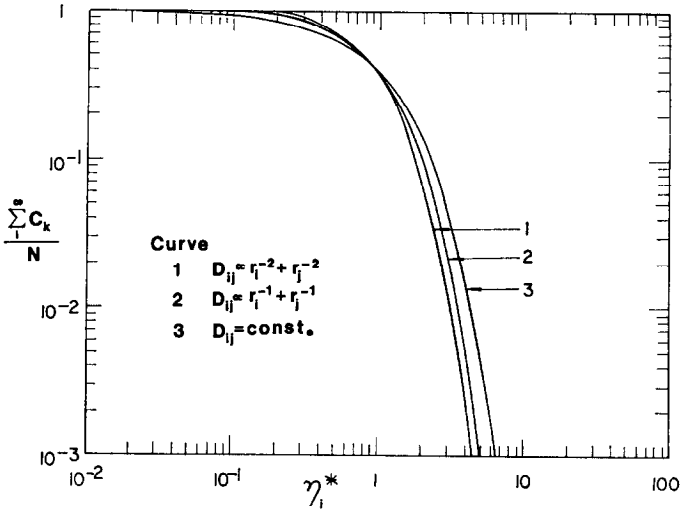

FIG. 4. Cumulative distribution for diffusion controlled case.

In Fig. 4 the cumulative distribution is plotted for various size dependencies of the diffusion coefficient as a function of η_i^*. For sintering control and an initially unisized distribution, Fig. 5 shows that in the N_v/N, η_i^* representation a family of curves characterized by various values of τ_1 is obtained. The curves from Figs. 4 and 5 show important differences over the whole size range of crystallites and thus allow differentiation between diffusion and sintering control. Because the theoretical curves in Fig. 4 are so close to each other, no information concerning the size dependence of the diffusion coefficient can be obtained.

In what follows it will be shown that some global characteristics, for instance the variance, allow identification of the rate determining step of the aging process.

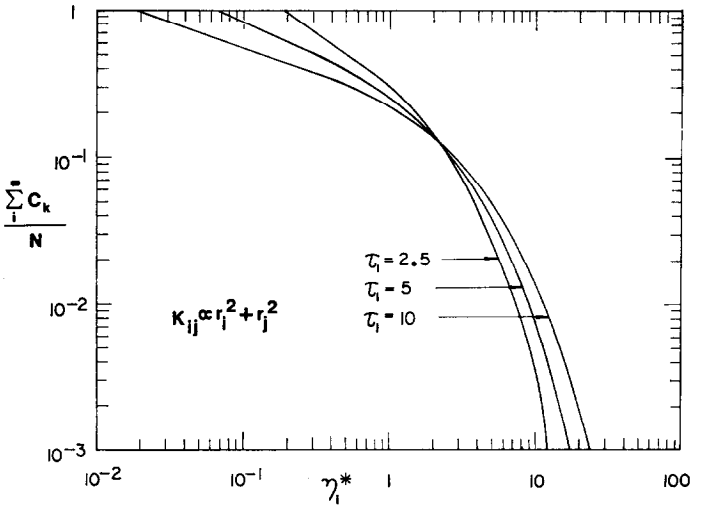

FIG. 5. Cumulative distribution for sintering controlled case; unisized initial distribution.

2. *The Variance of the Size Distribution Used to Identify the Rate Determining Step*

The variance of the size distribution is defined by

$$\sigma^2 = \int_0^\infty (r - \langle r\rangle)^2 \frac{n(r)}{N}\, dr = \langle r^2\rangle - \langle r\rangle^2, \tag{7}$$

where

$$\langle r\rangle = \frac{1}{N}\int_0^\infty rn(r)dr \tag{8}$$

and

$$\langle r^2\rangle = \frac{1}{N}\int_0^\infty r^2 n(r)dr. \tag{9}$$

If the volume is assumed to be proportional to r^3, i.e., $v = kr^3$, and the similarity variables defined by Eqs. (1) and (2) are used, Eq. (7) leads for the standard deviation σ to

$$\sigma = (\langle r^2\rangle - \langle r\rangle^2)^{1/2} = \frac{\phi^{1/3}}{k^{1/3}N^{1/3}}[\mu_{2/3} - (\mu_{1/3})^2]^{1/2} \tag{10}$$

and Eq. (8) leads for the average radius $<r>$ to

$$\langle r\rangle = \frac{\phi^{1/3}\int_0^\infty \eta^{1/3}\psi\, d\eta}{k^{1/3}N^{1/3}} = \frac{\phi^{1/3}}{k^{1/3}N^{1/3}}\mu_{1/3}, \tag{11}$$

where the moments μ_m are defined by

$$\mu_m = \int_0^\infty \eta^m \psi\, d\eta. \tag{12}$$

The ratio between the average radius and the standard deviation permits elimination of the unknown proportionality constant k:

$$\frac{\langle r\rangle}{\sigma} = \frac{\mu_{1/3}}{[\mu_{2/3} - (\mu_{1/3})^2]^{1/2}}. \tag{13}$$

For diffusion control the ratio $<r>/\sigma$ attains, after a short transient period, a constant value. For sintering control, after a short period of strong time dependence, this ratio becomes a weakly dependent function of time (Fig. 6). In Fig. 6 the symbol $<L>$ rather than $<r>$ was chosen because Eq. (13) is valid for any characteristic dimension of the particle related to the volume via an expression of the form $v = kL^3$.

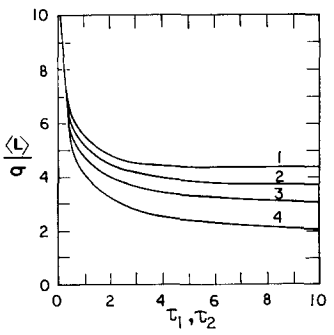

FIG. 6. The ratio of the average crystallite dimension $\langle L\rangle$ to the standard deviation σ as a function of the dimensionless times τ_1 and τ_2 for diffusion and sintering control, unisized initial distribution. (1) $K_{ij} \propto r_i^{-2} + r_j^{-2}$; (2) $K_{ij} \propto r_i^{-1} + r_j^{-1}$; (3) K_{ij} = const.; (4) $K_{ij} \propto r_i^2 + r_j^2$.

Table 1 contains the values of the moments, μ_m. For diffusion controlled aging, various size dependencies of the diffusion coefficient are considered. For sintering controlled aging, the values of the moments are given for $\alpha_{ij} \propto [(r_i^2 + r_j^2)/(r_i + r_j)]$ and an initially unisized distribution. Values for all the moments of importance in any of the experimental methods discussed in this paper are included.

For diffusion controlled aging, and depending on the size dependence of the diffusion coefficient, the mean dimension $<L>$ is related to the standard deviation σ by

$$\langle L\rangle = 4.36\sigma \text{ for } \left(D_{ij} \propto \frac{1}{r_i^2} + \frac{1}{r_j^2}\right),$$

$$\langle L\rangle = 3.70\sigma \text{ for } \left(D_{ij} \propto \frac{1}{r_i} + \frac{1}{r_j}\right),$$

$$\langle L\rangle = 2.76\sigma \text{ for } (D_{ij} = \text{const}).$$

For sintering control (see Fig. 6)

$$\langle L\rangle = 2.41\sigma \quad \text{for } \tau_1 = 5,$$

$$\langle L\rangle = 2.06\sigma \quad \text{for } \tau_1 = 10.$$

The values given for sintering control have been obtained for an initially unisized dis-

TABLE 1

VALUES OF THE MOMENTS μ_m OF THE SIZE DISTRIBUTION SPECTRUM ψ

		$\mu_{-2/3}$	$\mu_{-1/3}$	μ_0	$\mu_{1/3}$	$\mu_{2/3}$	μ_1	$\mu_{4/3}$	$\mu_{5/3}$	μ_2	$\mu_{7/3}$	$\mu_{8/3}$
Diffusion control $\mu_m = \int_0^\infty \eta^m \psi(\eta) d\eta$												
Assumed size dependence of D_{ij}												
$D_{ij} \propto \frac{1}{r_i^2} + \frac{1}{r_j^2}$		1.304	1.109	1.	0.952	0.954	1.	1.093	1.241	1.461	1.775	2.221
$D_{ij} \propto \frac{1}{r_i} + \frac{1}{r_j}$		1.476	1.159	1.	0.935	0.938	1.	1.122	1.320	1.619	2.059	2.709
$D_{ij} = \text{const.}$		2.679	1.354	1.	0.893	0.903	1.	1.191	1.505	2.000	2.778	4.012
Sintering control $\mu_m = \int_0^\infty \eta^m \psi(\eta, \tau_1, \phi^* = 1) d\eta$												
Assumed size dependence of α_{ij}	Dimensionless time τ_1[a]											
$\alpha_{ij} \propto \frac{r_i^2 + r_j^2}{r_i + r_j}$	2.5	1.847	1.297	1.	0.869	0.869	1.	1.305	1.896	3.000	5.09	9.1
	5	2.897	1.571	1.	0.792	0.799	1.	1.477	2.467	4.493	8.79	18.3
	7.5	4.142	1.833	1.	0.737	0.752	1.	1.598	2.895	5.749	12.26	27.7
	10	5.553	2.085	1.	0.695	0.718	1.	1.688	3.232	6.764	15.32	37.0

[a] At $\tau_1 = 0$ the distribution was unisized.

tribution (this kind of distribution appears to be valid for certain fresh metal catalysts). For other initial distributions, different values will be obtained for $<L>/\sigma$. However, in all cases a broad size distribution will develop after sufficient heating, and consequently the ratio $<L>/\sigma$ will decrease. Figure 7 compares the theoretical predictions with the experimental data for supported metal catalysts (*3, 4, 8*).

Figure 7 includes experimental results on the behavior of islands of metal on the surface of an amorphous support (*9, 10*). Skofronick *et al.* (*9, 10*) studied the structural changes of vacuum-deposited gold islands on amorphous supports of carbon and silicon monoxide undergoing additional heat treatment. They found that: (a) the number of islands per unit area of support decreased; (b) the mean radius and the standard deviation increased; and (c) the fraction of the support area covered by the islands decreased. Since the growth mechanism is as for supported metal catalysts, it is natural to include the data in Fig. 7. Figure 7 shows that identification of the rate determining mechanism and of the size dependence of the diffusion coefficient is indeed possible. The representation used in Fig. 7 is valid only after the effect of the initial distribution has disappeared: For diffusion control the universal $(\psi-\eta)$ curve is then attained; for sintering control the size distributions get broader with time of heat treatment and thus the ratio $\sigma/<L>$ increases with time. After sufficiently long heat treatment, the experimentally obtained ratio $\sigma/<L>$ will lie above the region for diffusion control and will move to even higher $\sigma/<L>$ ratios after additional heat treatment.

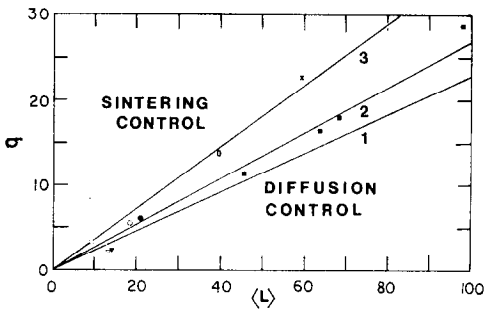

FIG. 7. The standard deviation σ as a function of the average crystallite dimension $\langle L \rangle$ as obtained from theoretical predictions and as observed experimentally for supported metal catalysts and islands of metal on thin films. (○) reduced at 500°C, impregnation type (*4*); (●) reduced at 600°C, impregnation type (*4*); (▽) reduced at 500°C, adsorption type (*4*); (▼) reduced at 770°C, adsorption type (*4*); (□) reduced at 470°C, impregnation type (*3*); (**O**) heated in vacuum, 15 hr (*8*); (**X**) heated in air, 15 hr (*8*); (■) gold islands on carbon and silicon monoxide supports (*10*). Sintering control above line (3); diffusion control below line (3); (1) $D_{ij} \propto r_i^{-2} + r_j^{-2}$; (2) $D_{ij} \propto r_i^{-1} + r_j^{-1}$; (3) $D_{ij} = \text{const.}$

3. *Electronmicroscopy Used to Determine the Magnitude of the Diffusion Coefficient and the Rate of Merging Constant*

Depending upon the rate determining step, the time dependence of the total number of particles now allows estimation of the magnitude of either the diffusion coefficient or of the rate-of-merging constant. It has been shown previously (*2*) that the rate of change of the total number of particles for diffusion control is given by:

$$\frac{dN}{dt} = -b_1 N^{2-m}, \tag{14}$$

where

$$b_1 = \frac{K^*}{2}\phi^m \int_0^\infty \int_0^\infty \psi(\eta)\psi(\tilde{\eta})(\tilde{\eta}^m + \eta^m)d\eta d\tilde{\eta}, \tag{15}$$

$$K^* = \frac{4\pi}{\ln(4T)} D_1 v_1^{-m}, \tag{16}$$

and

$$T = \frac{D_{11}\theta'}{R_{11}^2}. \tag{17}$$

Equation (14) is valid if $\ln 4T \gg 1$. Because K^* varies only slowly with θ' and thus with T, $\ln(4T)$ is henceforth assumed constant. Equation (14) allows computation of the ratio $D_1/\ln(4T)$. With an estimation of $\ln(4T)$, the diffusion coefficient is then obtained. The experimental data of Skofronick *et al.* (*9, 10*) for small gold

islands on a support—described above in some detail—are now used to compute the magnitude of the diffusion coefficient. From Fig. 7, where Skofronick's data are plotted, one may conclude that the size dependence of the diffusion coefficient is represented satisfactorily by $D_{ij} \propto (1/r_i) + (1/r_j)$, i.e., $m = -\frac{1}{3}$. Introducing $m = -\frac{1}{3}$ into Eq. (14) and integrating, one obtains with $\mu_{-1/3} = 1.159$ (see Table 1)

$$\frac{D_1}{\ln(4T)} = \frac{3\phi^{1/3}}{16\pi v_1^{1/3} 1.159(t_2 - t_1)} \times \left[\frac{1}{N_2^{4/3}} - \frac{1}{N_1^{4/3}}\right]. \quad (18)$$

Equation (18) allows computation of the ratio $D_1/\ln(4T)$ from experimental data.

For Skofronick's data the ratio $D_1/\ln(4T)$ varies, depending on the experimental conditions, between 3×10^{-16} and 1.5×10^{-17} cm²/sec (assuming $r_1 = 10$ Å). To obtain the diffusion coefficient D_1 from the ratio $D_1/\ln(4T)$, the quantity $\ln(4T) = \ln(4D_{11}\theta'/R_{11}^2)$ has to be estimated. The small scale time θ' is, however, not provided by the theory. Because the time θ' influences the diffusion coefficient only via $\ln\theta'$, even large changes in the value of θ' have a weak effect on the value of the diffusion coefficient. For a specific example [Expt 8, Table 2 in (*10*)] the ratio $D_1/\ln(4T)$ is computed from Eq. (18), and one obtains $D_1/\ln(4T) = 2.45 \times 10^{-16}$ cm²/sec. Choosing 100 sec $< \theta' <$ 9000 sec, where 9000 sec is the total time of the experiment, one obtains for $r_1 = 10$ Å that D_1 is in the range of 2×10^{-15} to 6×10^{-16} cm²/sec. Using the same procedure, one finds that, depending upon experimental conditions, the diffusion coefficient of the gold islands in Skofronick's experiments is of the order of 10^{-15} to 5×10^{-17} cm²/sec. For supported metal catalysts, we previously (*2*) have computed a diffusion coefficient of the same order of magnitude.

If the aging process is sintering controlled, the rate of merging constant, α_{11}, can be obtained as follows:

For sintering control, the rate of change of the total number of particles is given by (*1*, *2*)

$$\frac{dN}{dt} \approx -b_1 N^{2-m}, \quad (19)$$

where

$$b_1 = K^* \phi^m \mu_m, \quad (20)$$

$$K^* = \frac{2\pi r_1 \alpha_{11}}{v_1^m}, \quad (21)$$

and

$$\mu_m = \int_0^\infty \psi(\eta, \tau_1, \phi^*) \eta^m d\eta. \quad (22)$$

In the derivation of Eq. (19), the size dependence of the rate of merging constant, α_{ij}, is assumed to be of the form

$$\alpha_{ij} = C \frac{r_i^{3m} + r_j^{3m}}{r_i + r_j}. \quad (23)$$

The time dependence of μ_m is weak compared to the time dependence of N (see App. A), and thus b_1 can be considered constant. Equation (19) can thus be integrated to yield an expression for the rate of merging constant α_{11}:

$$\alpha_{11} = \frac{v_1^m}{(1-m)(t_2 - t_1)\phi^m \mu_m 2\pi r_1} \times \left[\frac{1}{N_2^{1-m}} - \frac{1}{N_1^{1-m}}\right] \text{ for } m \neq 1 \quad (24)$$

and

$$\alpha_{11} = \left(\log\left(\frac{N_1}{N_2}\right)\right) \frac{v_1}{(t_2 - t_1)\phi 2\pi r_1} \text{ for } m = 1. \quad (25)$$

N_1 and N_2 are the total number of particles at times t_1 and t_2, respectively. The exponent m may be found from the rate of change of the total number of particles in the system. The moments μ_m are of order unity. For $m = \frac{2}{3}$ the appropriate moments are given in Table 1. Equations (24) or (25) thus allow estimation of the rate-of-merging constant α_{11}.

No experimental data obtained by electron microscopy are available to compute α_{11}. However, as shown below, data obtained with other techniques are available and will be used to compute the rate-of-merging constant α_{11}.

III. X-Ray Line Broadening

X-Ray line broadening is extensively used to determine the particle sizes of supported metal crystallites in the size range 50–500 Å. The mean dimension, L, of the crystallites composing the sample, is related to the X-ray diffraction broadening, β, by (*11*, *12*)

$$L = \frac{K_L \lambda}{\beta \cos \theta},$$

where L is the mean crystallite dimension, λ the wavelength of the X-rays, θ the Bragg angle, β the diffraction line breadth after correction (see below), and K_L depends on the definition of the mean crystallite dimension L, the definition of the line breadth β, the shape of the crystallites, and the reflection plane considered. For details about the application of X-ray line broadening to supported metal catalysts see Refs. (*12–23*).

1. Comments About the Mean Dimension Measured by X-Ray Line Broadening

It is commonly accepted in the catalysis literature that X-ray line broadening gives the mean length of the crystallite size distribution defined by (*24–28*)

$$L_w = \frac{\int_0^\infty n(l) l^4 dl}{\int_0^\infty n(l) l^3 dl}. \tag{26}$$

This conclusion is based on the work of Jones (*14*) who considered the broadening caused by the size distribution of cubic crystals. Assuming that the total intensity reflected by the crystal is proportional to its volume, Jones obtained for the integral breadth β of the diffraction

$$\beta = \frac{\lambda}{\cos \theta [\Sigma_1^\infty n_i(l_i) l_i^4 / \Sigma_1^\infty n_i(l_i) l_i^3]}.$$

More recent investigations have shown that this result cannot be generalized to arbitrary reflection planes and crystallite shapes. A more general treatment, based on the work of Stokes and Wilson (*29*), and Bertraut (*30*), leads to the following expression for the integral breadth β (*31*, *32*)

$$\beta = \frac{\lambda}{L \cos \theta}. \tag{27}$$

In Eq. (27) the effective particle dimension L is given by the expression

$$L = \frac{\iint T_{xy}^2 dx dy}{\iint T_{xy} dx dy}, \tag{28}$$

where T_{xy} is the crystal dimension in the direction perpendicular to the considered reflecting plane x–y. The integration in Eq. (28) is carried out over all the particles in the sample. These equations are valid for a dilute ensemble of particles of arbitrary shape, randomly oriented.

The dimension L in Eq. (28) represents a volume average of the distribution of crystallites normal to the reflecting plane, i.e.,

$$L = \frac{1}{V} \int T dV = \langle T^2 \rangle / \langle T \rangle, \tag{28a}$$

Schwarz inequality (see App. B for details) shows that $<T^2>$ is equal or larger than $<T>^2$ and consequently L is equal or larger than $<T>$.

Let us consider the case in which line broadening is caused by a distribution, n_i, of small cubic crystallites of sizes L_i, the sides of which are parallel to the axis of the cubic crystallite. Assume that the reflecting plane is parallel to one of the sides of the cube. The integration in Eq. (28) can be carried out in a simple manner, and one obtains Jones' result:

$$L = \frac{\iint T_{xy}^2 dx dy}{\iint T_{xy} dx dy} = \frac{\Sigma_1^\infty n_i(L_i) L_i^4}{\Sigma_1^\infty n_i(L_i) L_i^3}. \tag{26}$$

For arbitrary crystal shapes and reflection planes, the dimension L obtained from X-ray line broadening, Eq. (28), does not reduce to Eq. (26). Furthermore, it is difficult to obtain experimentally the integral breadth, since it is difficult to evaluate the area in the tails of the reflection profile. The half maximum intensity breadth, defined as the breadth at half the maximum intensity, is usually measured instead. However, a general expression for the half maximum intensity breadth similar to Eqs. (27) and (28) cannot usually be derived.

One may conclude that X-ray line

broadening yields a mean average of the crystallite dimension normal to the reflecting plane [Eq. (28)], which only in the special case of cubes, and when certain reflection planes are considered, reduces to the mean dimension usually used in catalysis [Eq. (26)]. Also the integral breadth, rather than the half maximum intensity breadth, has to be measured.

In principle it is possible to calculate the particle size distribution from the peak shape of the diffraction line (*31*). However, for supported metal catalysts it is difficult to obtain an accurate corrected peak shape.

2. *Time Dependence of the Mean Average Crystallite Dimension Used to Identify the Rate Determining Step of the Aging Process*

The time dependence of the mean average crystallite dimension, regardless of its exact definition may allow identification of the rate determining step in the aging process. In App. A it is shown that the time dependence of the average particle size, defined by the general expression

$$R_{e,f} = \left[\frac{\int_0^\infty r^e n(r,t)dr}{\int_0^\infty r^f n(r,t)dr}\right]^{1/(e-f)} \qquad (29)$$

is given by

$$(R_{e,f})^{3(1-m)} = C_1 t + C_2$$

for diffusion control, and by

$$R_{e,f} \approx C_3 t + C_4$$

for sintering control ($m = \frac{2}{3}$).

Provided the mean average crystal dimension obtained from X-ray line broadening can be equated to the average radius, $R_{e,f}$, the above equations can be used to determine both the aging mechanism and the size dependence of the diffusion coefficient.

IV. Small Angle X-Ray Scattering

Investigations of metal dispersions of supported metal catalysts with small angle X-ray scattering technique (SAXS) have been made only seldom because the scattering from the pores of the support and the crystallites contained in them are correlated. Consequently the scattering from the pores cannot be treated as part of the background and substracted out. The scattering from the pores, however, can be eliminated, either by filling the pores with a liquid of the same electron density as the support (*33*) or by destroying the pores by pressure sintering the catalyst sample prior to the small angle scattering experiment (*34*). SAXS was recently used for platinum metal dispersions on alumina (*34–36*) and for platinum metal dispersions on charcoal catalysts (*37*). Whyte *et al.* (*35, 38*) eliminated the interfering scattering from the micropores of the alumina support by filling the pores with small amounts of CH_2I_2 or C_4H_9I. Somorjai *et al.* (*34*) reduced the pore scattering by pressure sintering the catalyst sample. Parlitz *et al.* (*37*) assumed that the effect of the metal crystallites can be obtained substracting the scattering of the blank support. Since no additivity of the scattering of metal and support exists, their results have to be reconsidered.

The theoretical equations concerning the intensity of the scattered X-ray (*39–44*) allow determination of two average radii, the Guinier radius (radius of gyration), R_G, and the Porod radius, R_P. For a point-shaped X-ray beam

$$R_G^2 = \frac{\int_0^\infty n(r)r^8 dr}{\int_0^\infty n(r)r^6 dr} = \frac{\langle r^8\rangle}{\langle r^6\rangle}, \qquad (30)$$

and

$$R_P = \frac{\int_0^\infty n(r)r^3 dr}{\int_0^\infty n(r)r^2 dr} = \frac{\langle r^3\rangle}{\langle r^2\rangle}. \qquad (31)$$

For a line-shaped beam

$$R_{G_L}^2 = \langle r^7\rangle/\langle r^5\rangle \qquad (32)$$

and

$$R_{P_L} = \frac{\langle r^3\rangle}{\langle r^2\rangle}. \qquad (33)$$

In what follows it is shown that as soon as the similarity representation becomes valid, the ratio R_P/R_G is a constant for diffusion controlled aging. After an initial

strong variation, the same ratio becomes a weakly dependent function of time for sintering controlled aging. Comparison of the experimentally obtained and computed values of this ratio allows identification of the rate controlling step of the process.

1. The Ratio R_P/R_G Used to Identify the Rate Determining Step

Since the available experimental data have been obtained with a line-shaped X-ray beam, only R_{GL} and R_{PL} are considered in the following treatment. If the volume is assumed proportional to r^3, $v = kr^3$, (k = const.), and if the similarity variables (1) and (2) are introduced one can write

$$R_{GL} = \frac{1}{k^{1/3}} \left(\frac{\int_0^\infty v^{7/3} n(v) dv}{\int_0^\infty v^{5/3} n(v) dv} \right)^{1/2} = \frac{\phi^{1/3}}{k^{1/3} N^{1/3}} \left(\frac{\int_0^\infty \eta^{7/3} \psi d\eta}{\int_0^\infty \eta^{5/3} \psi d\eta} \right)^{1/2} \quad (34)$$

and

$$R_{PL} = \frac{1}{k^{1/3}} \frac{\int_0^\infty v n(v) dv}{\int_0^\infty v^{2/3} n(v) dv} = \frac{\phi^{1/3}}{k^{1/3} N^{1/3} \int_0^\infty \eta^{2/3} \psi d\eta}. \quad (35)$$

Dividing Eq. (35) by Eq. (34) leads to the elimination of the unknown proportionality constant k. One obtains

$$\frac{R_{PL}}{R_{GL}} = \frac{(\int_0^\infty \eta^{5/3} \psi d\eta)^{1/2}}{\int_0^\infty \eta^{2/3} \psi d\eta (\int_0^\infty \eta^{7/3} \psi d\eta)^{1/2}}. \quad (36)$$

Because for diffusion control ψ depends after a short time only on η, the ratio R_{PL}/R_{GL} is a constant, the value of which depends on the size dependence of the diffusion coefficient of the crystallites.

For sintering control the ratio R_{PL}/R_{GL} is plotted in Fig. 8 as a function of τ_1. Until $\tau_1 \approx 5$, the mentioned ratio has a rapid variation, while for larger values of τ_1 the variation is weaker.

Table 2 gives the theoretical values obtained for the ratio R_{PL}/R_{GL} for diffusion control and sintering control. The moments of the similarity distribution used in the calculations are listed in Table 1. The ratio R_{PL}/R_{GL} is a measure of the width of the distribution function $n(v)$.

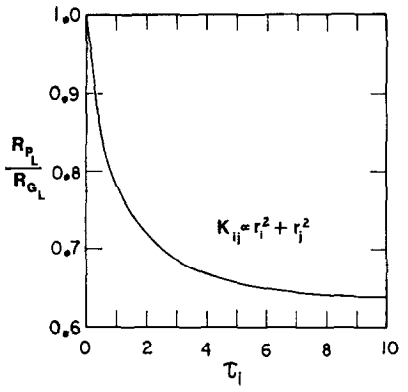

FIG. 8. The ratio of the Porod radius to the Guinier radius for a line-shaped X-ray beam from numerical solution of kinetic equations for sintering control; unisized initial distribution.

For diffusion control with strongly size dependent diffusion coefficients, the distribution function is relatively narrow. This fact is indicated here by a ratio R_{PL}/R_{GL} close to 1. For diffusion control with size independent diffusion coefficient, the distribution function is less narrow, while for sintering control the distribution function is very broad and its breadth increases with time.

Table 3 lists the results of Whyte *et al.* (*35*) for platinum dispersion on alumina and shows that the rate of aging was sintering controlled in all cases.

TABLE 2
THE RATIO R_{PL}/R_{GL} FOR VARIOUS MECHANISMS AS OBTAINED FROM THE THEORY

	R_{PL}/R_{GL}
Diffusion control	
$D_{ij} \propto \frac{1}{r_i^2} + \frac{1}{r_j^2}$	0.877
$D_{ij} \propto \frac{1}{r_i} + \frac{1}{r_j}$	0.853
D_{ij} = const.	0.815
Sintering control[a]	
$\tau_1 = 2.5$	0.702
$\tau_1 = 5$	0.662
$\tau_1 = 7.5$	0.647
$\tau_1 = 10$	0.640

[a] At $\tau_1 = 0$ unisized distribution.

TABLE 3
EXPERIMENTAL RESULTS OF WHYTE *et al.* (*35*)

Catalyst	$2R_{G_L}$	$2R_{P_L}$	R_{P_L}/R_{G_L}
F-G (fresh)	57	37	0.649
A-G (aged)	75	56	0.747
F-3 (fresh)	59	41	0.695
A-3 (aged)	64	43	0.672

2. *The Time Dependence of R_G Used To Calculate the Rate of Merging Constant*

In App. A it is shown that for diffusion control and $D_{ij} \propto (1/r_i^2) + 1/(r_j^2)$, R_G^5 is a linear function of time

$$R_G^5 = C'_1 t + R_{G_0}^5. \tag{37}$$

For sintering control and $m = \frac{2}{3}$, R_G is in good approximation a linear function of time

$$R_G \approx C_3 t + R_{G_0}. \tag{38}$$

Somorjai *et al.* (*34*) have measured R_{G_L} as a function of time for platinum on alumina in both reducing and oxidizing atmospheres. They found:

a. That a faster change occurred at higher temperatures,

b. That heating in an oxidizing atmosphere caused a faster growth process than heat treatment in a reducing atmosphere,

c. That the samples exhibited a very fast growth in the first few hours, which leveled off with time.

The effect of the temperature and of the atmosphere have been explained in our previous paper (*2*) by their influence on the mobility of the crystallites and on the merging behavior of the crystallites. The growth behavior can be explained as follows. Initially the crystallites are small and their mobility is relatively high, so that their growth is controlled by the merging process of the crystallites. Figure 9 shows the experimental dependence of the average radius of gyration as a function of time during the initial period. In the cases for which enough experimental information is available, R_G is a linear

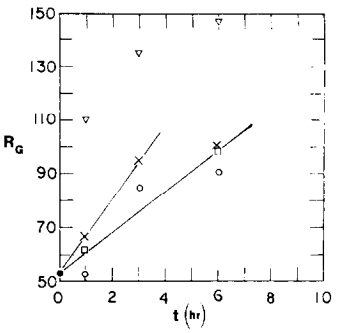

FIG. 9. The time dependence of the Guinier radius as observed experimentally (*34*). Oxidizing atmosphere: (▽) $T = 700$°C; (□) $T = 600$°C; reducing atmosphere: (×) $T = 700$°C; (○) $T = 600$°C. (●) Guinier radius at $t = 0$ in all the cases.

function of time to a good approximation. This kind of dependence shows that the rate of aging is sintering controlled during this period.

After extended heat treatment, the crystallites have grown appreciably and their mobility is decreased. Additional restrictions are caused by the fact that some of the crystallites are now of the same order of magnitude as the pores in which they lodge and consequently their diffusion is hindered.

In what follows, the rate of change of the Guinier radius, R_G, during the initial period of Somorjai's experiments is used to compute the magnitude of the merging constant α_{11}.

Because (see App. A)

$$R_G \approx C_3 t + R_{G_0}, \tag{39}$$

where

$$C_3 = \frac{b_1 \phi^{1/3}}{3k^{1/3}} \left[\frac{\mu_{8/3}}{\mu_2}\right]^{1/2},$$

$$b_1 = K^* \phi^{2/3} \mu_{2/3},$$

and

$$K^* = \frac{2\pi r_1 \alpha_{11}}{v_1^{2/3}},$$

the rate of merging constant, α_{11}, may be shown to be given by

$$\alpha_{11} = \frac{3r_1 k(R_G - R_{G_0})}{2\pi\phi t} \frac{1}{\mu_{2/3}} \left(\frac{\mu_2}{\mu_{8/3}}\right)^{1/2}. \tag{40}$$

Assuming that the particles are spheres and the surface area of the support is of the order of 200 m^2/g of support, the rate of merging constant, α_{11}, for two particles of radius 10 Å is obtained as:

$\alpha_{11} \approx 2.1 \times 10^{-9}$ cm/sec for 600°C and in an oxidizing atmosphere;

$\alpha_{11} \approx 1.8 \times 10^{-9}$ cm/sec for 600°C and in a reducing atmosphere;

$\alpha_{11} \approx 4. \times 10^{-9}$ cm/sec for 700°C, again in a reducing atmosphere.

We previously (*2*) have computed for the rate-of-merging constant for $Pt-Al_2O_3$ reforming catalysts values of the same order of magnitude.

V. Magnetic Measurements

This method, which is applicable for ferromagnetic metals, for example nickel, cobalt, and iron yields two average volumes of the particle size distribution, the low field volume v_{LF} and the high field volume v_{HF}. For details on this method see Refs. (*45–49*). The low field volume v_{LF} and the high field volume v_{HF} are defined by

$$v_{LF} = \frac{\langle v^2 \rangle}{\langle v \rangle} = \frac{\int_0^\infty v^2 n(v) dv}{\int_0^\infty v n(v) dv}, \tag{41}$$

$$v_{HF} = \langle v \rangle = \int_0^\infty v n(v) dv. \tag{42}$$

Using the similarity variables (1) and (2) these equations can be rewritten as

$$v_{LF} = \frac{\phi}{N} \int_0^\infty \eta^2 \psi d\eta \tag{43}$$

and

$$v_{HF} = \frac{\phi}{N}. \tag{44}$$

If the volume is assumed proportional to r^3, i.e., $v = kr^3$, a low field radius, R_{LF}, and a high field radius, R_{HF}, may be calculated as

$$R_{LF} = \frac{1}{k^{1/3}} \frac{\phi^{1/3}}{N^{1/3}} \left(\int_0^\infty \eta^2 \psi d\eta \right)^{1/3} \tag{45}$$

and

$$R_{HF} = \frac{1}{k^{1/3}} \frac{\phi^{1/3}}{N^{1/3}}. \tag{46}$$

The high field radius is independent of the form of the size distribution and thus independent of the aging mechanism. The ratio R_{LF}/R_{HF} is given by

$$\frac{R_{LF}}{R_{HF}} = \left(\int_0^\infty \eta^2 \psi d\eta \right)^{1/3}. \tag{47}$$

For diffusion control this ratio is a constant, the value of which depends on the size dependence of the diffusion coefficient. Using the appropriate moments (see Table 1), one obtains from Eq. (47)

$$\frac{R_{LF}}{R_{HF}} = 1.13 \qquad \left(D_{ij} \propto \frac{1}{r_i^2} + \frac{1}{r_j^2} \right),$$

$$\frac{R_{LF}}{R_{HF}} = 1.17 \qquad \left(D_{ij} \propto \frac{1}{r_i} + \frac{1}{r_j} \right),$$

$$\frac{R_{LF}}{R_{HF}} = 1.26 \qquad (D_{ij} = \text{const.}).$$

For sintering control the ratio R_{LF}/R_{HF} is plotted in Fig. 10 as a function of τ_1. For $\tau_1 = 10$, R_{LF}/R_{HF} has a value of 1.89 and will move to still higher values for increasing τ_1. Comparison of Fig. 10 with the values obtained for diffusion control shows that the value of the ratio of R_{LF}/R_{HF} allows identification of the rate determining step. For diffusion control, the size dependence of the diffusion coefficient, however, cannot be determined since the

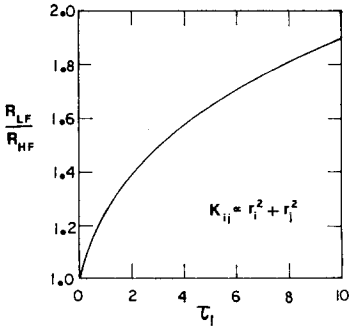

Fig. 10. The ratio of the low magnetic field radius to the high magnetic field radius from numerical solution of kinetic equations for sintering control; unisized initial distribution.

obtained values are too close to each other. Reinen and Selwood (*47*) have obtained saturation magnetizations for nickel supported on silica gel and on γ-alumina for both fresh and thermally treated (sintered) catalysts. For the sintered catalyst only the low field radius was obtained. For the fresh nickel silica coprecipitate and the nickel alumina impregnate, however, both low field and high field radii are reported [(*47*), Table 1]. Since during the preparation of these samples, high temperatures were used for extended times, migration and sintering of the unreduced nickel may already have occurred. One thus might expect that even the fresh catalysts may already follow the unique curve.

The ratio R_{LF}/R_{HF} yields:

$$R_{LF}/R_{HF} = \frac{23}{15} \approx 1.53 \qquad \text{for nickel–silica coprecipitate}$$

and

$$R_{LF}/R_{HF} = \frac{26}{13} = 2 \qquad \text{for nickel–alumina impregnate.}$$

Such a high ratio of R_{LF}/R_{HF} indicates that the agglomeration during the preparation process was sintering controlled.

VI. Chemisorption Measurements of the Exposed Surface Area of Metal

Dynamic and static chemisorption methods discussed in several review papers (*8, 38, 50–56*) are available. Though the dynamic methods are easily applicable, the gas uptake cannot be related in a simple way to the surface area of the sample. Consequently the discussion will be restricted here to the static methods. If one assumes that the particles have a similar shape, the specific surface area S^* per gram of metal is related to the average particle dimension l_{vs}

$$S^* = \frac{1}{\rho}\frac{\alpha_s}{\alpha_v}\frac{1}{l_{vs}}, \tag{48}$$

where ρ is the density of the metal, α_s the surface shape factor, α_v the volume shape factor and

$$l_{vs} = \frac{\int_0^\infty n(l)l^3dl}{\int_0^\infty n(l)l^2dl}. \tag{49}$$

For spheres and cubes having all surfaces exposed $\alpha_s/\alpha_v = 6$, while the linear dimension l_{vs} is the diameter of the sphere and the length of the cube, respectively.

In what follows the time dependence of the exposed surface area of metal per unit area of support, S, is used to determine the rate determining step of the aging process. S^* and S are related by a constant factor, dependent on the metal loading of the catalyst and the surface area of the support.

1. *The Time Evolution of the Exposed Metal Surface Area Used to Identify the Rate Determining Step*

It has been shown previously (*1, 2*) that for rate constants of the form

$$K(v,\tilde{v}) = K^*(\tilde{v}^m + v^m) \tag{50}$$

the time dependence of the exposed surface area S of the metal is given by

$$\frac{dS}{dt} = -b_3S(t)^{4-3m}, \tag{51}$$

where

$$b_3 = \frac{K^*}{3\phi^{2-3m}b_2{}^{3-3m}}\frac{\mu_m}{\mu_{2/3}{}^{3-3m}}. \tag{52}$$

b_2 is a geometric factor, dependent on the shape of the particles which is related to the surface and volume shape factors by

$$b_2 = \frac{\alpha_s}{\alpha_v{}^{2/3}}. \tag{53}$$

For diffusion control the coefficient b_3 is after a certain time (in which the similarity solution is reached) independent of time. For sintering control b_3 is after an initial rapid variation with time a weakly dependent function of time. For the particular value, $m = \frac{2}{3}$, Eq. (52), reduces, for sintering control, to the constant

$$b_3 = \frac{K^*}{3b_2}. \tag{54}$$

Integration of Eq. (51) leads to

$$\left(\frac{S_0}{S}\right)^{3-3m} = 1 + S_0{}^{3-3m}b_3t \tag{55}$$

for diffusion control, and to

$$\left(\frac{S_0}{S}\right) = 1 + S_0 b_3 t \qquad (56)$$

for sintering control if $m = 2/3$.

If for sintering control $m \neq 2/3$, Eq. (55) remains approximately valid because the coefficient b_3 has a much weaker time dependence than the exposed surface area S.

The decay of the exposed surface area is very sensitive to the rate determining step of the aging process. In the case of sintering control, when $m = 2/3$, $1/S$ increases linearly with time, while in the diffusion controlled range, $(1/S)^{3-3m}$ increases linearly with time. For example, for a diffusion coefficient which depends on size as $D_i \propto r_i^{-2}$, $(1/S)^5$ increases linearly with time.

In our previous paper [(2), Table 1] we have used this high sensitivity of the decay of the exposed surface area to determine the mechanism of the aging process and the size dependence of the diffusion coefficient for a variety of Pt-on-alumina catalysts.

VII. Comparison of the Various Methods

Each of the discussed techniques provides an average radius of the size distribution of the crystallites summarized in Table 4.

The only radius which is independent of the form of the size distribution is the high magnetic field radius

$$R_{HF} = \frac{1}{k^{1/3}} \frac{\phi^{1/3}}{N^{1/3}}.$$

In Table 5 this radius is chosen as 100, and the other average radii obtained from the different experimental methods and for different aging mechanisms are compared to R_{HF}. The average radii were computed using the appropriate equations given in the text together with the values for the moments of the similarity distribution listed in Table 1.

For diffusion control with a strongly size dependent diffusion coefficient, the size distribution is narrow and consequently the values of the average radii are close to each other, within 20%. For sintering control the size distribution becomes very broad with time and the average radii vary by more than a factor of 2.

For both diffusion control and sintering control, the relationship among the average radii can be described by inequalities of the form

$$R_{HF} \leq R_{VS} = R_P \leq R_W \leq R_{LF} \leq R_G. \qquad (57)$$

TABLE 4

Average Volumes as Measured by the Different Techniques

Method	Average volume
X-ray line broadening[a]	$v_W = kR_W^3 = \frac{(\int_0^\infty v^{4/3} n(v,t)dv)^3}{(\int_0^\infty v n(v,t)dv)^3}$
Gas-chemisorption method	$v_{VS} = kR_{VS}^3 = \frac{(\int_0^\infty v n(v,t)dv)^3}{(\int_0^\infty v^{2/3} n(v,t)dv)^3}$
Small angle X-ray scattering	$v_{G_L} = kR_{G_L}^3 = \frac{(\int_0^\infty v^{7/3} n(v,t)dv)^{3/2}}{(\int_0^\infty v^{5/3} n(v,t)dv)^{3/2}}$
	$v_P = kR_P^3 = \frac{(\int_0^\infty v n(v,t)dv)^3}{\int_0^\infty (v^{2/3} n(v,t)dv)^3}$
Magnetic measurements	$v_{LF} = \frac{\int_0^\infty v^2 n(v,t)dv}{\int_0^\infty v n(v,t)dv}$
	$v_{HF} = \frac{\int_0^\infty v n(v,t)dv}{\int_0^\infty n(v)dv}$
Electron microscopy provides any average volume needed	

[a] As defined by Eq. (26).

TABLE 5

THEORETICAL PREDICTIONS OF THE RELATIVE MAGNITUDE OF THE AVERAGE RADII OBTAINED BY VARIOUS METHODS FOR DIFFUSION AND SINTERING CONTROL

	R_{HF}	R_P	R_{VS}	R_W[a]	R_{LF}	R_{G_L}	R_G
Diffusion control							
$D_{ij} \propto r_i^{-2} + r_j^{-2}$	100	105	105	109	113	120	123
$D_{ij} \propto r_i^{-1} + r_i^{-1}$	100	107	107	112	117	125	129
D_{ij} = const.	100	111	111	119	126	136	147
Sintering control (initially unisized)							
$\tau_1 = 2.5$	100	115	115	131	144	164	175
$\tau_1 = 5$	100	125	125	148	165	189	202
$\tau_1 = 7.5$	100	133	133	160	179	205	220
$\tau_1 = 10$	100	139	139	169	189	218	234

[a] As defined by Eq. (26).

The equal signs associated with the inequality signs are only valid for unisized distributions. In App. B it is shown that these inequalities, Eq. (57), are valid for all possible size distributions.

By using two different experimental methods, the inequalities may be used for checking the accuracy of both the basic assumptions of the methods and the accuracy of the experimental procedure.

The literature is rich in data reported for crystallite sizes obtained simultaneously with more than one method.

In Table 6 some of these results are summarized and compared to the inequalities (Eq. 57). In the cases where the experimental data do not satisfy the inequalities, possible explanations are advanced.

APPENDIX A

The time dependence of certain average radii of the distribution function can be obtained starting from the general expression

$$R_{e,f} = \left[\frac{\int_0^\infty r^e n(r,t)dr}{\int_0^\infty r^f n(r,t)dr}\right]^{1/(e-f)} \cdot \quad \text{(A-1)}$$

The volume is assumed to be proportional to r^3, $v = kr^3$. Using the similarity variables ψ and η, one obtains

$$R_{e,f} = \frac{\phi^{1/3}}{k^{1/3}} N^{-1/3} \left[\int_0^\infty \eta^{e/3}\psi d\eta \int_0^\infty \eta^{f/3}\psi d\eta\right]^{1/e-f} \cdot \quad \text{(A-2)}$$

The rate of change of the total number of particles, N, is given by Eqs. (14) and (19) for diffusion control and for sintering control, respectively. Integrating Eq. (14), one obtains for diffusion control

$$\left(\frac{N_0}{N}\right)^{1-m} = 1 + (1-m)N_0^{1-m}b_1 t. \quad \text{(A-3)}$$

For sintering control and $m = \frac{2}{3}$, b_1 in Eq. (19) is a weakly dependent function of time (see Fig. 11). Since the total num-

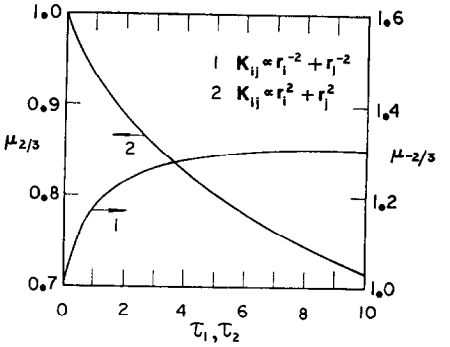

FIG. 11. The moments $\mu_{2/3}$ for sintering control and $\mu_{-2/3}$ for diffusion control as a function of τ_1 and τ_2 obtained from numerical solution of kinetic equations, unisized initial distribution.

ber of particles, N, changes much faster with time than b_1, one can integrate Eq. (19) assuming that b_1 is constant. One obtains

$$\left(\frac{N_0}{N}\right)^{1/3} \approx 1 + \frac{1}{3} N_0^{1/3} b_1 t. \qquad \text{(A-4)}$$

Figure 12 compares the total number of particles obtained numerically by solving the exact discrete version of the population balance [Eq. (2) in (*2*)] with that obtained from Eqs. (A-3) and (A-4). Using Eq. (A-3), Eq. (A-2) becomes

$$(R_{e,f})^{3(1-m)} = C_1 t + C_2 \quad \text{(diffusion control)}, \qquad \text{(A-5)}$$

where

$$C_1 = \frac{b_1(1-m)}{k^{1-m}} \phi^{1-m} \left[\int_0^\infty \eta^{e/3} \psi(\eta) d\eta \Big/ \int_0^\infty \eta^{f/3} \psi(\eta) d\eta \right]^{3(1-m)/e-f}$$

and

$$C_2 = \frac{C_1}{(1-m) b_1 N_0^{1-m}}$$

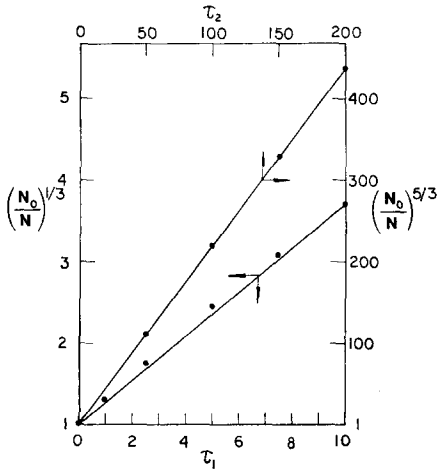

FIG. 12. Comparison of the total number of crystallites for sintering and diffusion control obtained from numerical solution of kinetic equations with those obtained from Eqs. (A-3) and (A-4). (●) Numerical solution of population balance; (—) Eqs. (A-3) and (A-4).

For sintering control and $m = \frac{2}{3}$, one obtains

$$R_{e,f} \approx C_3 t + C_4, \qquad \text{(A-6)}$$

where

$$C_3 = \frac{b_1 \phi^{1/3}}{3k^{1/3}} \left[\int_0^\infty \eta^{e/3} \psi(\eta,\tau_1,\phi^*) d\eta \Big/ \int_0^\infty \eta^{f/3} \psi(\eta,\tau_1,\phi^*) d\eta \right]^{1/e-f}$$

and

$$C_4 = \frac{3C_3}{b_1 N_0^{1/3}}.$$

APPENDIX B

From the numerical results given in Table 5 it results that

$$R_{\mathrm{HF}} \leq R_{\mathrm{VS}} = R_P \leq R_W \leq R_{\mathrm{LF}} \leq R_{GL}. \qquad \text{(B-1)}$$

In what follows it is shown that these inequalities hold for all possible size distributions. For convenience we use the average volumes rather than radii (between them the relation $v = kR^3$ is assumed valid). The inequalities (B-1) can be written as

$$v_{\mathrm{HF}} \leq v_{\mathrm{VS}} = v_P \leq v_W \leq v_{\mathrm{LF}} \leq v_{GL}. \qquad \text{(B-2)}$$

The following dimensionless quantities are introduced

$$g(x,t) = \frac{v_0}{N} n(v,t) \qquad \text{(B-3)}$$

and

$$x = \frac{v}{v_0}, \qquad \text{(B-4)}$$

where v_0 is the initial mean volume of the crystallites, i.e., $v_0 = \phi/N_0$.

The zeroth order moment of $g(x)$, M_0, and the first order moment of $g(x)$, M_1, are defined by

TABLE 6

AVERAGE CRYSTALLITE DIAMETERS (Å) OBTAINED BY VARIOUS TECHNIQUES

Catalyst, preparation, treatment and ref.	Chemisorption	X-Ray line broadening	Electron microscopy	Small angle X-ray scattering	Magnetic measurements	Comments
2.5% Pt/SiO_2 Impregnation Fresh catalyst (*24*)	34.4	37.9	$\frac{\Sigma n_i d_i^3}{\Sigma n_i d_i^2} = 30.5$ $\frac{\Sigma n_i d_i^4}{\Sigma n_i d_i^3} = 31.5$			—[f]
1.% Pt/Al_2O_3–SiO_2 Fresh catalyst (*8*)	53	47	50			—[g]
Thermal treatment in vacuum at 800°C, 15 hr (*8*)	53	46	49			—[g]
Air 800°C, 15 hr (*8*)	194	65	75			—[h]
3.0% Pt/SiO_2 Impregnation Fresh catalyst (*60*)	45	60	$\frac{\Sigma n_i d_i^3}{\Sigma n_i d_i^2} = 55$ $\frac{\Sigma n_i d_i^4}{\Sigma n_i d_i^3} = 65$[a]			—[i]
2.8% Pt/SiO_2 Impregnation Fresh catalyst reduced at 600°C (*4*)	30	32 (27% of Pt detected)	26[b]			—[j]
2.8% Pt/SiO_2 Impregnation Fresh catalyst reduced at 500°C (*4*)	16	27 (40% of Pt detected)	21[b]			—[j]
3.6% Pt/SiO_2 Adsorption Fresh catalyst reduced at 770°C (*4*)	30	15	16[b]			—[k]
5% Pd/kieselguhr Commercial catalyst sample (*26*)	112	163 (±30)		$\frac{\Sigma n_i d_i^3}{\Sigma n_i d_i^2} = 108$ $\frac{\Sigma n_i d_i^4}{\Sigma n_i d_i^3} = 154$		—[l]

10% Ni/Al_2O_3-SiO_2				$\left(\frac{\Sigma n_i d_i^6}{\Sigma n_i d_i^3}\right)^{1/3} \approx 30$	—[m]
Sintered at 370°C in H_2 (*61*)	77	<40			
Impregnation					—[m]
Sintered at 700°C in H_2 (*61*)	305	88			
0.62% Pt/Al_2O_3	81		$\frac{\Sigma n_i d_i^3}{\Sigma n_i d_i^2} = 56$		—[n]
Aged in commercial use					
Commercial catalyst sample (*35*)			$\left(\frac{\Sigma n_i d_i^7}{\Sigma n_i d_i^5}\right)^{1/2} = 75$		
0.35% Pt/Al_2O_3	18		$\frac{\Sigma n_i d_i^3}{\Sigma n_i d_i^2} = 43$		—[o]
Aged in commercial use (*35*)			$\left(\frac{\Sigma n_i d_i^7}{\Sigma n_i d_i^5}\right)^{1/2} = 64$		
25.5% Ni/SiO_2				$\left(\frac{\Sigma n_i d_i^6}{\Sigma n_i d_i^3}\right)^{1/3} = 23$	—[p]
Coprecipitation (*47*)				$(\Sigma n_i d_i^3)^{1/3} = 15$	
13.5% Ni/Al_2O_3				$\left(\frac{\Sigma n_i d_i^6}{\Sigma n_i d_i^3}\right)^{1/3} = 26$	—[p]
Impregnation (*47*)				$(\Sigma n_i d_i^3)^{1/3} = 13$	
58.5% Ni/kieselguhr	90[d]	70[c]	$\frac{\Sigma n_i d_i^3}{\Sigma n_i d_i^2} = 47$[c]		—[q]
(*28*)	109[e]		$\frac{\Sigma n_i d_i^4}{\Sigma n_i d_i^3} = 60$[c]		
3.1% Pt/Al_2O_3	253	255			—[r]
Impregnation					
Heat treated 24 hr 750°C (*16*)					
4.46% Pt/Al_2O_3	212	255			—[r]
Impregnation					
Heat treated 24 hr 650°C (*16*)					
0.6% Pt/Al_2O_3	61	200			—[s]
Impregnation					
Heat treated 2 hr 650°C (*16*)					

(*Continued*)

TABLE 6 (*Continued*)

[a] Summation over crystallites 50 Å and above.

[b] Crystallite diameter defined such that half the surface area stems from crystallites of this size or smaller.

[c] Reduced at 310°C.

[d] Reduced at 350°C.

[e] Reduced at 450°C.

[f] Because the two averages obtained by electron microscopy are very near to each other, the particle size distribution is narrow; the chemisorption average and the first electron microscopy average are defined in the same manner and thus have to lead to the same value; the differences appear to be within experimental confidence limits.

[g] Narrow particle size distribution; inequalities (56) not satisfied; however the differences are within experimental confidence limits.

[h] The averages obtained by X-ray line broadening and electron microscopy are in agreement; the average obtained by chemisorption does not satisfy inequalities (56) probably because a fraction of the metal surface is inaccessible to the adsorbate due to partial collapse of the support during heating.

[i] Ineuqalities satisfied, not too broad size distribution; differences for the same kind of average crystallite diameter are within experimental confidence limits.

[j] Narrow particle size distribution; inequalities (56) between chemisorption average and X-ray line broadening satisfied; the electron microscopy average is not directly comparable with other averages due to its definition.

[k] The value obtained by chemisorption does not satisfy inequalities (56), probably because a part of the metal surface becomes inaccessible to the chemisorbing gas.

[l] Inequalities (56) satisfied; the size distribution is relatively broad.

[m] Inequalities (56) are not satisfied by the chemisorption radius, probably because a large fraction of the metal surface is inaccessible to the adsorbate.

[n] Agreement with inequalities (56) between the values obtained by small angle X-ray scattering; the size distribution is relatively broad; too high value obtained from chemisorption probably due to partial collapse of the support.

[o] Agreement with inequalities (56) for small angle X-ray scattering data; the too small value obtained from chemisorption measurements as compared to the small-angle X-ray data may be explained as follows: The small-angle X-ray method gives particle rather than crystallite sizes; these particles may be composed of several not completely sintered crystallites leaving additional area for chemisorption.

[p] Agreement with inequalities (56).

[q] Agreement with inequalities (56) for X-ray line broadening and electron microscopy averages; the chemisorption averages are too high; the chemisorption averages depend on the reduction temperature, namely they are larger for higher reduction temperatures.

[r] Agreement with inequalities (56); narrow particle size distribution.

[s] Inequalities (56) are satisfied; the large difference between the averages obtained by X-ray line broadening and chemisorption may be explained by the fact that only large crystallites are detected by the X-ray method used in Ref. (*16*).

$$M_0 = \int_0^\infty g(x,t)dx = 1, \quad \text{(B-5)}$$

$$M_1 = \int_0^\infty xg(x,t)dx = \frac{N_0}{N} \equiv a \geq 1. \quad \text{(B-6)}$$

The variance σ^{*2} of the dimensionless size distribution $g(x,t)$ is related to the moments M_1 and M_2 via

$$\sigma^{*2} = M_2 - M_1^2 = M_2 - a^2. \quad \text{(B-7)}$$

For $M_0 = 1$, $M_1 = a$ and $M_2 = \sigma^{*2} + a^2$ the following inequalities have been established by Von Mises (*62*)

$$a^x\left(1 + \frac{\sigma^{*2}}{a^2}\right)^{x-1} < M_x < a^x \quad \text{if } 0 < x < 1, \quad \text{(B-8)}$$

$$a^x < M_x < a^x\left(1 + \frac{\sigma^{*2}}{a^2}\right)^{x-1} \quad \text{if } 1 < x < 2, \quad \text{(B-9)}$$

$$M_x > a^x\left(1 + \frac{\sigma^{*2}}{a^2}\right)^{x-1} \quad \text{if } x > 2. \quad \text{(B-10)}$$

These inequalities result from the Schwarz inequality together with the assumptions that $P(x,t) = \int_0^x g(x,t)\,dx$ is an increasing function of x in the interval $0 \leq x \leq \infty$, and that $\lim_{b\to 0} \int_0^b g(x,t)\,dx = 0$.

Using Eq. (B-8) for $x = \frac{2}{3}$, it may be shown that

$$\frac{M_2}{a} > \frac{a^3}{M_{2/3}^3} > a$$

or

$$v_{LF} > v_{VS} = v_P > v_{HF}. \quad \text{(B-11)}$$

Inequality (B-9) leads for $x = \frac{4}{3}$ to

$$a < \frac{M_{4/3}^3}{a^3} < \frac{M_2}{a}$$

or

$$v_{LF} > v_W > v_{HF}. \quad \text{(B-12)}$$

Inequality (B-10) leads for $x = \frac{7}{3}$ to

$$M_{7/3} > \frac{M_2^{4/3}}{a^{1/3}}. \quad \text{(B-13)}$$

Inequality (B-9) yields, for $x = \frac{5}{3}$,

$$a^{5/3} < M_{5/3} < a^{1/3}M_2^{2/3}. \quad \text{(B-14)}$$

With $v_G/v_0 = (M_{7/3}/M_{5/3})^{3/2}$, and Eqs. (B-13) and (B-14) one can show that

$$\frac{v_G}{v_0} > \frac{M_2}{a},$$

or

$$v_{GL} > v_{LF}. \quad \text{(B-15)}$$

Equations (B-11), (B-12) and (B-15) are equivalent to Eq. (B-2), provided that $v_W/v_P > 1$.

From Table 4 it follows

$$\frac{x_W}{x_P} = \frac{M_{4/3}^3 M_{2/3}^3}{a^6}.$$

Making use of the Schwarz inequality

$$\left[\int_0^\infty f_1(x)f_2(x)g(x)dx\right]^2 \leq \left[\int_0^\infty f_1^2(x)g(x)dx\right]\left[\int_0^\infty f_2^2(x)g(x)dx\right], \quad \text{(B-16)}$$

with $f_1(x) = x^{2/3}$ and $f_2(x) = x^{1/3}$ it results

$$M_{4/3}M_{2/3} \geq a^2 \quad \text{(B-17)}$$

and thus

$$v_W \geq v_P. \quad \text{(B-18)}$$

Consequently the inequalities (B-2) and (B-1) hold for all possible size distributions.

Acknowledgment

Acknowledgment is made to the donors of the Petroleum Research Fund, administered by the American Chemical Society, for support of this research.

References

1. Ruckenstein, E., and Pulvermacher, B., *AIChE J.* **19**, 356 (1973); Errata in *AIChE J.* **19**, 1286 (1973).
2. Ruckenstein, E., and Pulvermacher, B., *J. Catal.* **29**, 224 (1973).
3. Wilson, G. R., and Hall, W. K., *J. Catal.* **17**, 190 (1970).
4. Wilson, G. R., and Hall, W. K., *J. Catal.* **24**, 306 (1972).
5. Pestridge, E. B., and Yates, D. J. C., *Nature (London)* **234**, 345 (1971).

6. Botty, M. C., Davies, M. C., and Felton, C. D., *Anal. Chem.* **36,** 173 R (1964).

7. Zaidman, N. M., Dzisko, V. A., Karnautkhov, A. P., Kefeli, L. M., Krasilenko, N. P., Koroleva, N. G., and Ratner, I. D., *Kinet. Katal.* **10,** 386 (1969).

8. Spindler, H., *Z. Chem.* **13,** 1 (1973).

9. Skofronick, J. G., and Phillips, W. B., *J. Appl. Phys.* **38,** 4791 (1967).

10. Phillips, W. B., Desloge, E. A., and Skofronick, J. G., *J. Appl. Phys.* **39,** 3210 (1968).

11. Scherrer, P., *Göttinger Nachrichten* **2,** 98 (1918).

12. Klug, H. P., and Alexander, L. E., "X-Ray Diffraction Procedures," Wiley, London, 1954.

13. Warren, B. E., *J. Appl. Phys.* **12,** 375 (1941).

14. Jones, F. W., *Proc. Roy. Soc. Ser. A* **166,** 16 (1938).

15. Van Nordstrand, R. A., Lincoln, A. J., and Carnevale, A., *Anal. Chem.* **36,** 830 (1964).

16. Spenadel, L., and Boudart, M., *J. Phys. Chem.* **64,** 204 (1960).

17. Herrmann, R. A., Adler, S. F., Goldstein, M. S., and De Baun, R. M., *J. Phys. Chem.* **65,** 2189 (1961).

18. Spindler, H., and Baginski, K., *Chem. Tech. (Leipzig)* **20,** 548 (1968).

19. Spindler, H., and Kraft, M., *Z. Anorg. Chem.* **391,** 155 (1972).

20. Avery, N. R., and Sanders, J. V., *J. Catal.* **18,** 129 (1970).

21. Plank, C. J., Kokotailo, G. T., and Drake, L. C., Joint Symp. Div. Petrol. Chem., Coll. and Surf. Chem., 140th Amer. Chem. Soc. Meet., Chicago, 16-I (1960).

22. Mills, G. A., Weller, S., and Cornelius, E. B., *Actes Congr. Int. Catal. 2nd, 1960* **2,** 2221 (1961).

23. McHenry, K. W., Bertolacini, R. J., Brennan, H. M., Wilson, J. L., and Seelig, H. S., *Actes Congr. Int. Catal., 2nd, 1960* **2,** 2295 (1961).

24. Adams, C. R., Benesi, H. A., Curtis, R. M., and Meisenheimer, R. G., *J. Catal.* **1,** 336 (1962).

25. Pope, D., Smith, W. L., Eastlake, M. J., and Moss, R. L., *J. Catal.* **22,** 72 (1971).

26. Scholten, J. J. F., and Van Monfoort, A., *J. Catal.* **1,** 85 (1962).

27. Van Hardeveld, R., and Van Monfoort, A., *Surface Sci.* **4,** 396 (1966).

28. Geus, J. W., and Nobel, A. P. P., *J. Catal.* **6,** 108 (1966).

29. Stokes, A. R., and Wilson, A. J. C., *Proc. Cambridge Phil. Soc.* **38,** 313 (1942).

30. Bertraut, E. F., *Acta Crystallogr.* **3,** 14 (1950).

31. Warren, B. E., "X-Ray Diffraction," Addison-Wesley, Reading, MA, 1969.

32. Buchanan, D. R., McCullough, R. L., and Miller, R. L., *Acta Crystallogr.* **20,** 922 (1966).

33. Gunn, E. L., *J. Phys. Chem.* **62,** 928 (1958).

34. Somorjai, G. A., Powell, R. E., Montgomery, P. W., and Jura, G., *in* "Small Angle X-Ray Scattering" (H. Brumberger, Ed.), p. 449. Gordon and Breach, New York, 1967.

35. Whyte, Jr., T. E., Kirklin, P. W., Gould, R. W., and Heinemann, H., *J. Catal.* **25,** 407 (1972).

36. Chu, B., *J. Phys. Chem.* **67,** 1916 (1963).

37. Parlitz, B., Schnabel, K. H., Sarachow, A. I., Plavnik, G. M., and Dubinin, M. M., *Z. Anorg. Allg. Chem.* **389,** 43 (1972).

38. Whyte, T. E., Jr., *Catal. Rev.* **8,** 117 (1973).

39. Hosemann, R., *Z. Phys.* **113,** 751 (1939).

40. Riseman, J., *Acta Crystallogr.* **5,** 193 (1952).

41. Guinier, A., and Fournet, G., "Small-Angle Scattering of X-Rays." Wiley, London, 1955.

42. Baur, R., and Gerold, V., *Acta Met.* **12,** 1449 (1964).

43. Porod, G., *Kolloid.-Z.* **124,** 83 (1951); **125,** 51, 109 (1952).

44. Schmidt, P. W., and Hight, R., Jr., *Acta Crystallogr.* **13,** 480 (1960).

45. Selwood, P. W., "Adsorption and Collective Paramagnetism." Academic Press, New York, 1962.

46. Bean, C. P., and Livingston, J. D., *J. Appl. Phys.* **30,** 120S (1959).

47. Reinen, D., and Selwood, P. W., *J. Catal.* **2,** 109 (1963).

48. Neugebauer, C. A., *J. Appl. Phys.* **31,** 152S (1960).

49. Abeledo, C. R., and Selwood, P. W., *J. Appl. Phys.* **32,** 229S (1961).

50. Gil'debrand, E. I., *Int. Chem. Eng.* **6,** 449 (1966).

51. Sinfeld, J. H., *Chem. Eng. Progr., Symp. Ser.* **63,** 16 (1967).

52. Schlosser, E. G., *Chem.-Ing. Tech.* **39,** 409 (1967).

53. Gregg, S. J., and Sing, K. S. W., "Adsorption, Surface Area and Porosity," Chap. 6. Academic Press, London, 1967.

54. Boudart, M., *in* "Advances in Catalysis" (D. D. Eley, H. Pines and P. B. Weisz, Eds.), Vol. 20, p. 153. Academic Press, New York, 1969.

55. Muller, J., *Rev. Pure Appl. Chem.* **19,** 151 (1969).

56. CINNEIDE, A. D. O., AND CLARKE, J. K. A., *Catal. Rev.* **7,** 213 (1972).

57. KARNAUKHOV, A. P., *Kinet. Katal.* **12,** 1520, (1971).

58. LYON, H. B., AND SOMORJAI, *J. Chem. Phys.* **46,** 2539 (1967).

59. MCLEAN, M., AND MYKURAJ, H., *Surface Sci.* **5,** 466 (1966).

60. Moss, R. L., *Platinum Metals Rev.* **11,** 141 (1967).

61. CARTER, J. L., CUSUMANO, J. A., AND SINFELT, J. H., *J. Phys. Chem.* **70,** 2257 (1966).

62. VON MISES, R., "Mathematical Theory of Probability and Statistics." Academic Press, New York, 1964.